

The nature of valley-spin filtering effect in transition metal dichalcogenide monolayers

Dominik Szcześniak^{1,2*} and Sabre Kais¹

¹ *Department of Chemistry, Purdue University, 560 Oval Dr.,
47907 West Lafayette, Indiana, United States of America and*

² *Department of Theoretical Physics, Faculty of Science and Technology,
Jan Długosz University in Częstochowa, 13/15 Armii Krajowej Ave., 42200 Częstochowa, Poland*

(Dated: December 21, 2024)

The magnetically-induced valley-spin filtering in transition metal dichalcogenide monolayers promises new paradigm in information processing. Herein, the mechanism of this effect is elucidated within the metal-induced gap states concept. The filtering is shown to be primarily governed by the valley-spin polarized tunnelling processes, which yield fundamental scaling trends for valley-spin selectivity with respect to the intrinsic physics of the filter materials. The results are found to facilitate insight into the analyzed effects and provide general design guidelines toward efficient valley-spin filter devices based on discussed materials or other hexagonal monolayers with broken inversion symmetry.

I. INTRODUCTION

Most of the present concepts behind the electronic control of information rely on the manipulation of charge flow or spin angular momentum of electrons. However, recent developments in quantum electronics show that it is also possible to address an alternative property of the electron, namely its valley pseudospin [1–6]. In comparison to its charge and spin counterparts, the valley degree of freedom constitute binary index for the low-energy electrons associated with the local conduction band minima (valleys) in the momentum space of a crystal [1]. As a result, it is expected that the valley-based (valleytronic) devices should provide new or improved functionalities in the field of classical and quantum information processing *e.g.* in terms of low-power valley or hybrid valley-spin logic devices [7–9] as well as complex qubit basis sets [9, 10]. Nonetheless, to efficiently perform valleytronic operations in solid state systems, it is required to have control over the selective population of distinguishable valleys, toward their polarization [3–6]. Moreover, the electrons should occupy polarized valleys long enough to allow logic operations of interest [8, 9].

Given the above background, not all solid state materials that exhibit local energy extrema in the momentum space are well suited for the valley control of information. From among the systems already considered as potential hosts for valleytronics [1, 2, 11–13], the most promising are the two-dimensional (2D) layered crystals with honeycomb structures, due to their strong valley-selective coupling with the external fields [8, 9]. In the family of such 2D systems, currently of particular attention are the group-VIB transition metal dichalcogenide monolayers (MX_2 , where M =Mo, W and X =S, Se, Te) [8]. Similar to the graphene, the MX_2 materials possess two inequivalent but energetically degenerate valleys at the K and K' high symmetry points in their first hexagonal Brillouin zone [14]. However, the MX_2 monolayers are also characterized by the inherently broken inversion symmetry

and the strong spin-orbit coupling (SOC). In what follows, they exhibit direct semiconducting band gaps and can benefit from the chiral optical selection rules toward dynamical control of the valley population [4, 15]. The same properties lead also to the coupling between the valley and spin degrees of freedom (the valley-spin locking) [16] and allow control of their polarization by the means of the out-of-plane external magnetic field [5, 17] or the magnetic exchange field [18, 19].

In terms of the information processing in MX_2 materials, the idea to manipulate valley pseudospin via the magnetic field effects appears so far to be more robust than use of the optical pumping methods [20, 21]. Although initial approaches struggled with the weak scaling of valley polarization as a function of the magnetic field strength, recent studies shows plausible possibility of using magnetic exchange fields to enhance valley splitting [18–20, 22]. Interestingly, this approach inspired also the early attempts aimed at electronic generation and control of valley carriers in selected MX_2 monolayers [6, 21, 23, 24]. Most importantly, however, the discussed method of control allows to utilize the MX_2 materials as a magnetic channel contacts between metallic leads (the so-called two-terminal setup) to perform valley- and spin-resolved switching operations, by the analogy to the well-established concept of the spin-filter [25, 26]. The described valley-spin filter received already notable consideration, initially in terms of the graphene-based systems [2, 3, 27, 28] and later based on the discussed here MX_2 monolayers [29–31]. However, although mentioned above studies provide successful initial modeling of the MX_2 valley-spin filters, the in-depth discussion of the underlying transport phenomena is still absent in the literature, hampering further developments in the field.

In this context, this study attempts to elucidate the mechanism of valley-spin filtering effect in MX_2 materials, by directly addressing its canonical nature. Such insight is meant to include, usually ignored, inherent and distinct electronic properties of the MX_2 materials *i.e.* their multiband structure with complex orbital symmetry behavior, the strong spin-orbit coupling, as well as the Berry curvatures. As a result, this analysis intends to

* dszczesn@purdue.edu; d.szczesniak@ujd.edu.pl

facilitate the fundamental understanding of the discussed processes and provide their general trends with respect to the pivotal control parameters such as the magnetic field strength, transport channel length and Fermi level position in the semiconductor. Hence, the results are expected to be of importance for the future design of valley-spin filter devices for information processing, as build by using the MX_2 monolayers or potentially other 2D hexagonal materials with broken inversion symmetry.

II. THEORETICAL MODEL

To understand the nature of the valley-spin filtering in MX_2 materials, it is proposed here that the filtering processes in the MX_2 two-terminal filter setup can be related to the interfacial physics of a bulk metal-semiconductor junction. In particular, according to Heine [32] and Tersoff [33], at the ideal bulk metal-semiconductor interface the propagating states in a metal extend into the decaying states localized within the forbidden energy region of a semiconductor. Interestingly, such metal-induced gap states (MIGS) are known to still have significant amplitude in the vicinity of the interface and allow to model number of the electronic processes in this region [34]. As shown by Kane [35], the phenomena of tunneling via semiconducting part of the junction is one of such processes, which can be directly associated with the decay characteristics of the MIGS. By the analogy, the MX_2 materials in the two-terminal filter setup act as a semiconducting transport channel for the valley-spin carriers. Due to the relatively short length of such channel and its semiconducting character, it can be expected that the biggest contribution to the overall transport processes comes from the tunneling electrons. Therefore, the MIGS can be viewed as a concept that potentially explains the valley-spin filtering effect in MX_2 materials. This suggestion is reinforced by the fact that the MIGS were recently found to exist in the band gaps of the MX_2 monolayers [36]. Moreover, it was proven that the same states explain interfacial physics related to the electronic charge injection from a metal into the MX_2 materials [37].

To verify the role of MIGS in the spin-valley filtering, their behavior in the momentum space should be analyzed. This can be done by solving the inverse eigenvalue problem (IEP) [34, 36], assuming that wavevector (\mathbf{k}) in a solid takes on complex values. The matrix form of the IEP can be written as:

$$(\mathbf{H}_i - \mathbf{H}_{i+1}\vartheta - \dots - \mathbf{H}_{i+j-1}\vartheta^{j-1} - \mathbf{H}_{i+j}\vartheta^j) \Psi = 0, \quad (1)$$

where \mathbf{H}_i and \mathbf{H}_{i+j} denote component Hamiltonian matrices for the origin i^{th} unit cell and its interactions with the neighboring cells, respectively. Moreover in Eq. (1), $\vartheta = e^{i\mathbf{k}\mathbf{R}}$ is the generalized Bloch phase factor for a given \mathbf{R} lattice vector, while Ψ stands for the wave function column vector. In case of the MX_2 materials, the lattice vector takes form $\mathbf{R} = \alpha\mathbf{a}_x + \beta\mathbf{a}_y$, where \mathbf{a}_x and \mathbf{a}_y

describe the primitive vectors of 2D hexagonal lattice, whereas α and β are integer values. According to that, $j' \in [1, 2, \dots, j-1, j]$, where $j = \alpha$ or β depend on the chosen crystal direction.

To account for all the important electronic properties of the MX_2 crystals, herein these materials are described within the following magnetized total Hamiltonian:

$$\mathbf{H} = \mathbf{H}_{TB} + \mathbf{H}_{SOC} + \mathbf{H}_B. \quad (2)$$

In Eq. (2), the \mathbf{H}_{TB} part stands for the 6×6 tight-binding Hamiltonian, which includes up to the third-nearest-neighbor interactions and is constructed within the $\{|d_{z^2}, \uparrow\rangle, |d_{xy}, \uparrow\rangle, |d_{x^2-y^2}, \uparrow\rangle, |d_{z^2}, \downarrow\rangle, |d_{xy}, \downarrow\rangle, |d_{x^2-y^2}, \downarrow\rangle\}$ minimal basis for the M -type atoms, as shown in [38]. Next, the $\mathbf{H}_{SOC} = \lambda\mathbf{L} \cdot \mathbf{S}$ is the intra-atomic SOC term, in which λ gives the spin-orbit coupling constant, whereas \mathbf{L} and \mathbf{S} are the orbital and spin angular momentum operators, respectively. Finally, the $\mathbf{H}_B = -\mu\sigma_z \otimes \mathbf{I}_{3 \times 3}$ describes the influence of the external magnetic field, which is perpendicular to the MX_2 plane. Therein, $\mu = g\mu_B\mathbf{B}$ is the Zeeman energy, where $g = 2$ is the gyromagnetic factor for the d -type orbitals, μ_B stands for the Bohr magneton, and \mathbf{B} is the magnetic field in Teslas. Moreover, in \mathbf{H}_B , the σ_z describes Pauli spin matrix, \otimes is the Kronecker product and $\mathbf{I}_{3 \times 3}$ stands for the 3×3 identity matrix. The tight-binding and λ parameters are adopted from [38].

Due to the specific symmetry-based character of the Hamiltonian (2), the IEP of Eq. (1) retains its general nonlinear form with respect to ϑ , and has to be solved by the linearization methods [37]. As a results, the IEP yields the pairs of spin-dependent ϑ and $1/\vartheta$ solutions, which are linked by the time-reversal symmetry for each of the distinct valleys at the K and K' high symmetry points, respectively. In this manner, the eigenvalues of IEP corresponds to the propagating states when $|\vartheta| = 1$ and to the decaying states when $|\vartheta| < 1$. The combination of such IEP solutions is referred here to as the complex band structure (CBS), employed to directly relate the tunneling processes across MX_2 monolayers to their intrinsic electronic properties.

III. NUMERICAL RESULTS

In Fig. 1, the CBS solutions under selected values of the out-of-plane magnetic field are depicted for the representative MoTe_2 (first row) and WTe_2 (second row) materials, which exhibit the strongest valley- and spin-related effects among the Mo- and W-based monolayers, respectively. The middle panel of each sub-figure presents the spin-dependent propagating states for $q = \text{Re}[\mathbf{k}]$ along the $K' - \Gamma - K$ path in the hexagonal Brillouin zone. These states capture the band-edge properties in the vicinity of the band gap *e.g.* the large spin splitting of the valence band due to the SOC. On the other hand, the left and right panel of each subfigure presents the respective spin-dependent gap states for $\kappa = \text{Im}[\mathbf{k}]$ at the K' and K

points. Herein, only the gap solutions with the smallest κ for each spin orientation are presented, by arguing the fact that they describe the most penetrating states within the gap, according to the corresponding decay of the wave function per unit cell as given by $e^{-\text{Im}[\kappa]a}$, where a is the lattice constant. Therefore, these are the states described by the the lowest decay rates (κ), or the longest decay lengths ($1/\kappa$), that can be interpreted as the MIGS and suppose to provide the major contribution to the tunneling processes of interest.

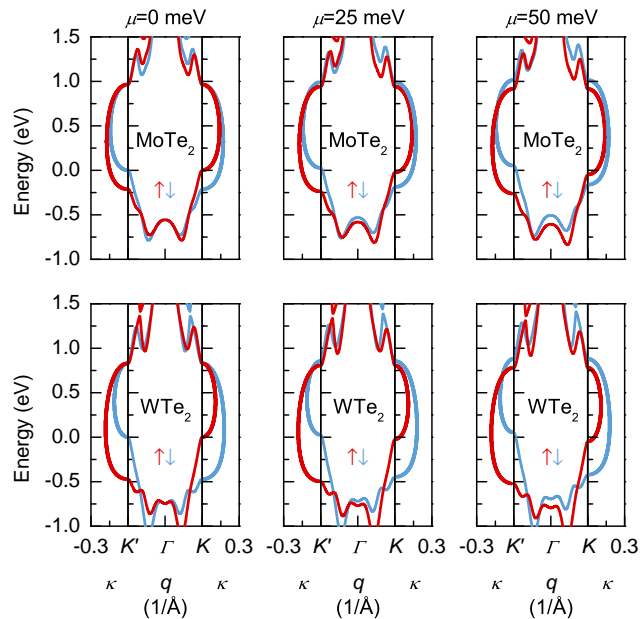


FIG. 1. The valley- and spin-resolved complex band structures of the MoTe₂ (first row) and WTe₂ (second row) monolayers for different values of the out-of-plane magnetic field (columns). The zero reference energy is set at the top-edge of the valence band, and the momentum axis is given in the unified unit of 1/Å.

In this context, the first observation arising from the presented results corresponds to the analytical character of the depicted decaying states, which visibly inherit spin properties of their propagating counterparts. Although less obvious, the discussed states also follow the orbital character of the propagating solutions. In particular, the orbital character of decaying states changes from the majority $d_{x^2-y^2}$ -type behavior in the vicinity of the donor-like valence band into the more d_{z^2} -type symmetry close to the acceptor-like conduction band. The change in the described orbital character occurs smoothly as the energy approaches the branch point of the semielliptic decaying state. In what follows, the decaying states clearly constitute the inherent property of the semiconductor and the direct continuum of the propagating states within the gap, in agreement with the MIGS character.

The results presented in Fig. 1 allow also to trace changes of the electronic behavior with respect to the applied out-of-plane magnetic field. In particular, the

propagating and decaying states respond in a conventional way to the Zeeman effect induced by the external magnetic field *i.e.* states with spins parallel to the field are lowered and those antiparallel raised in energies. Moreover, the relation between the total band gap values at the K ($E_G(K)$) and K' ($E_G(K')$) points is in good agreement with the experimental exciton charge measurements under out-of-plane magnetic field [17]. Yet, the most important observation is the relative shift in energies between the spin-dependent decaying states in the K and K' valleys, when the magnetic field takes on nonzero value. This fact qualitatively shows increasing valley- and spin-polarization of the MIGS with the growing magnetic field strength. This is to say, it suggest that the valley-spin filtering processes can be addressed within the concept of the MIGS.

To investigate this aspect further, it is first instructive to directly relate the MIGS to the tunneling probabilities. In reference to the mentioned above decay of the wavefunction within a semiconducting gap, the valley- and spin-dependent decay of the tunneling probabilities in the MX_2 -based filters can be given as $T_{K/K',\uparrow/\downarrow} = e^{-2\text{Im}[\kappa_{K/K',\uparrow/\downarrow}]L}$, where L is the length of the semiconducting channel. Note, that the tunneling probability decay should be calculated at the Fermi level to account for the dominant current contributions in the gap region. Herein, this level is not known *a priori*, since the metallic leads at the both ends of the semiconductor in the filter setup are not included explicitly in the present analysis. However, it is possible to set the canonical position of the Fermi level at the branch point of the decaying state characterized by the lowest κ value, by referring to the results presented previously for the Fermi level pinning phenomena at the metal- MX_2 junctions [37]. According to that, in the present analysis the reference level for the calculations is associated with the branch point of the spin-up MIGS in the K -valley (BP). Moreover, to account for the moderate Fermi level engineering two additional positions are considered, namely $\text{BP}^+ = \text{BP} + 0.25$ eV and $\text{BP}^- = \text{BP} - 0.25$ eV. In what follows it is possible now to investigate the total spin polarization:

$$P_S \equiv \frac{T_{K,\uparrow} - T_{K,\downarrow} + T_{K',\uparrow} - T_{K',\downarrow}}{T_{K,\uparrow} + T_{K,\downarrow} + T_{K',\uparrow} + T_{K',\downarrow}}, \quad (3)$$

as well as the corresponding total valley polarization:

$$P_V \equiv \frac{T_{K,\uparrow} + T_{K,\downarrow} - T_{K',\uparrow} - T_{K',\downarrow}}{T_{K,\uparrow} + T_{K,\downarrow} + T_{K',\uparrow} + T_{K',\downarrow}}. \quad (4)$$

In Fig. 2, the total spin and valley polarizations of the tunneling current decay in MX_2 monolayers are presented as a function of the out-of-plane magnetic field strength and the semiconducting channel length. The first row of subfigures corresponds to the solutions at the BP level, whereas next two rows refer to the results at the BP^+ and BP^- energies, respectively. Moreover, to cover conventional spatial sizes of the semiconducting channel in the tunnel filter setup, it is assumed that $L \in [1, 10]$ nm.

On the other hand $\mu \in [0, 70]$ meV, so that the BP^+ and BP^- levels are always within the energy gap range.

In general, the results presented in Fig. 2 show that the decay of tunneling currents in MX_2 crystals exhibits similar trends in terms of the valley and spin selectivity in a function of the external magnetic field and the channel length. In particular, the polarization of tunneling currents increases along with μ and L , although only the magnetic field allows to induce the polarization. Such growth of the P_S and P_V with the magnetic field strength can be associated with the Zeeman effect, by recalling described before behavior of the MIGS. On the other hand, the P_S and P_V increases in a function of the channel length, since higher values of L provide bigger contributions to the exponential form of $T_{K/K',\uparrow/\downarrow}$. Moreover, the polarization becomes stronger via given transition metal $\text{Mo} \rightarrow \text{W}$ and chalcogen $\text{S} \rightarrow \text{Se} \rightarrow \text{Te}$ substitutions, in accordance with the growing SOC constant in the corresponding monolayers. In general, the observed behavior proves that the valley- and spin-polarization of the MIGS is highly correlated according to the valley-spin locking in MX_2 materials. Most importantly however, presented results show that the MIGS describe the valley-spin filtering behavior in MX_2 monolayers, in agreement with the predictions made previously within computational modeling studies [21, 29–31].

In what follows, an additional observations can be made in regard to the efficiency of the valley-spin selectivity in MX_2 filters. Specifically, when the Fermi level is located at the midgap position the polarization is not impressive and reaches maximum of around 50%. However, the situation changes when its position is raised (BP^+) or lowered (BP^-) with respect to the BP energy, and in both cases leads to the substantial enhancement of the valley-spin selectivity in the tunneling processes. The location of the Fermi level closer to the valence band appears to be most beneficial and can be related to the strong SOC-derived spin splitting of the valence band. Finally, closer investigation of the results depicted in Fig. 2 allows to observe slightly different response of the P_S and P_V parameters to the increasing L value. This is especially visible when comparing results for the spin and valley polarization at the BP^+ energy level, since the MIGS with different spin and valley indices exhibit virtually the same κ values in the vicinity of the conduction band at $\mu = 0$. In a result, it can be argued that the discussed discrepancy is associated with the fact that P_S rely on the differences between the tunneling probability decay within the same valley, whereas P_V is defined for the decay processes in different valleys, therefore for the states related to each other by the time reversal symmetry.

IV. SUMMARY AND CONCLUSIONS

In summary, the conducted analysis shows that the mechanism of the valley-spin filtering effect in the MX_2

monolayers can be explained within the concept of the MIGS. This finding is of great importance to the future design of the MX_2 -based filter devices that employ valley and spin degrees of freedom for information processing, as it allows to explicitly relate the filtering processes of interest to the intrinsic electronic properties of the semiconducting channel. Moreover, the developed theoretical model allows to draw general trends in tuning the filtering properties with respect to the out-of-plane magnetic field strength, the semiconducting channel length, as well as the position of the Fermi level within the energy gap. The obtained filtering characteristics appears to be in agreement with the available computational modeling studies [21, 29–31], and should constitute relevant basis for further investigations aimed at the enhancement of valley and spin functionalities in low-dimensional systems. In particular, it is suggested that the best valley and spin selectivity under external magnetic field can be achieved for the Te-based monolayers if the Fermi level is located below the midgap position, according to the large spin splitting effect of the valence band. Note however, that the external magnetic field required for the valley and spin polarization is of the order of hundreds of Teslas, and the magnetic exchange fields should be considered as a practical polarization technique in this regard.

To this end, the presented theoretical analysis is expected to be of general benefit for the research on valley-spin dependent filtering in 2D materials. In particular, due to the properties of MX_2 materials and the universal character of MIGS concept, the reported results emerge as a case study of the valley-spin filtering processes in the entire class of the hexagonal monolayers with broken inversion symmetry. Simultaneously, the presented model holds also potential for explaining the valley-spin filtering in 2D materials when the polarization is induced and controlled by the non-magnetic means, as the MIGS are directly related to the band structure of a filter material.

V. ACKNOWLEDGEMENTS

D. Szcześniak acknowledges financial support of this work and the related research activities by the Polish National Agency for Academic Exchange (NAWA) under Bekker's programme (project no. PPN/BEK/2018/1/00433/U/00001). S. Kais would like to acknowledge funding by the U.S. Department of Energy (Office of Basic Energy Sciences) under award number DE-SC0019215. The Authors would like to also acknowledge fruitful discussions with Dr. Z. Hu (Purdue University).

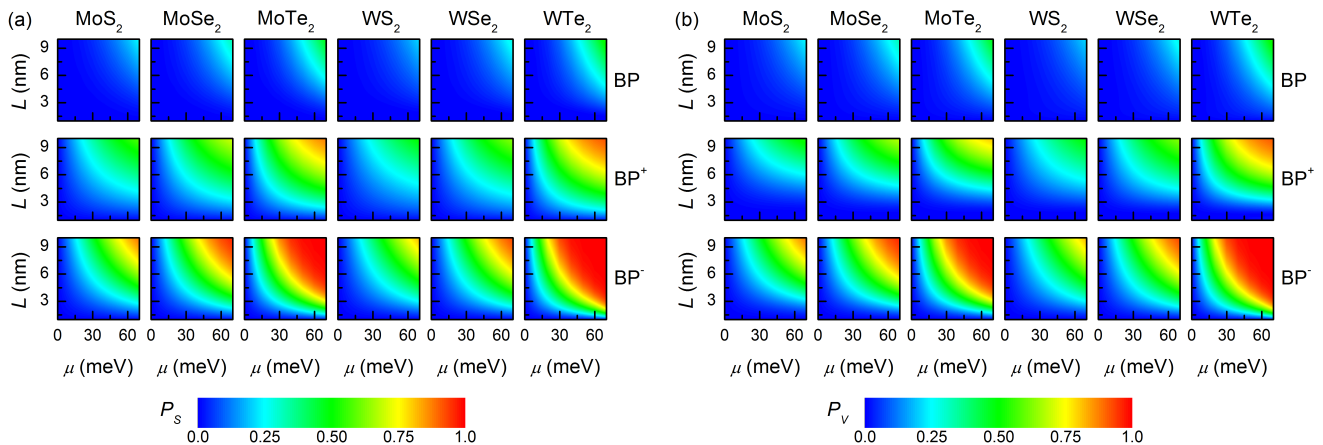


FIG. 2. The total spin (a) and valley (b) polarization of the tunneling probability decay in MX_2 monolayers as a function of the external magnetic field strength (μ) and semiconducting channel length (L). The results are depicted for three different positions of the Fermi level within the semiconducting band gap, from top to down for the BP, BP⁺, and BP⁻, respectively.

-
- [1] O. Gunawan, Y. P. Shkolnikov, K. Vakili, T. Gokmen, E. P. D. Poortere, and M. Shayegan, *Phys. Rev. Lett.* **97**, 186404 (2006).
- [2] A. Rycerz, J. Tworzydło, and C. W. J. Beenakker, *Nat. Phys.* **3**, 172 (2007).
- [3] D. Xiao, W. Yao, and Q. Niu, *Phys. Rev. Lett.* **99**, 236809 (2007).
- [4] K. F. Mak, K. He, J. Shan, and T. F. Heinz, *Nat. Nanotechnol.* **7**, 494 (2012).
- [5] G. Aivazian, Z. Gong, A. M. Jones, R. L. Chu, J. Yan, D. G. Mandrus, C. Zhang, D. Cobden, W. Yao, and X. Xu, *Nat. Phys.* **11**, 148 (2015).
- [6] Y. Ye, J. Xiao, H. Wang, Z. Ye, H. Zhu, M. Zhao, Y. Wang, J. Zhao, X. Yin, and X. Zhang, *Nat. Nanotechnol.* **11**, 598 (2016).
- [7] Y. S. Ang, S. A. Yang, C. Zhang, Z. Ma, and L. K. Ang, *Phys. Rev. B* **96**, 245410 (2017).
- [8] J. R. Schaibley, H. Yu, G. Clark, P. Rivera, J. S. Ross, K. L. Seyler, W. Yao, and X. Xu, *Nat. Rev. Mater.* **1**, 16055 (2016).
- [9] S. A. Vitale, D. Nezich, J. O. Varghese, P. Kim, N. Gedik, P. Jarillo-Herrero, D. Xiao, and M. Rothschild, *Small* **14**, 1801483 (2018).
- [10] N. Rohling and G. Burkard, *New J. Phys.* **14**, 083008 (2012).
- [11] K. Takashina, Y. Ono, A. Fujiwara, Y. Takahashi, and Y. Hirayama, *Phys. Rev. Lett.* **96**, 236801 (2006).
- [12] Z. Zhu, A. Collaudin, B. Fauqué, W. Kang, and K. Behnia, *Nat. Phys.* **8**, 89 (2012).
- [13] J. Isberg, M. Gabrysch, J. Hammersberg, S. Majdi, K. K. Kovi, and D. J. Twitchen, *Nat. Mater.* **12**, 760 (2013).
- [14] M. Chhowalla, H. S. Shin, G. Eda, L. J. Li, K. P. Loh, and H. Zhang, *Nat. Chem.* **5**, 263 (2013).
- [15] Z. Ye, D. Sun, and T. F. Heinz, *Nat. Phys.* **13**, 26 (2017).
- [16] D. Xiao, G. B. Liu, W. Feng, X. Xu, and W. Yao, *Phys. Rev. Lett.* **108**, 196802 (2012).
- [17] D. MacNeill, C. Heikes, K. F. Mak, Z. Anderson, A. Kormányos, V. Zólyomi, J. Park, and D. C. Ralph, *Phys. Rev. Lett.* **114**, 037401 (2015).
- [18] J. Qi, X. Li, Q. Niu, and J. Feng, *Phys. Rev. B* **92**, 121403 (2015).
- [19] C. Zhao, T. Norden, P. Zhang, P. Zhao, Y. Cheng, F. Sun, J. P. Parry, P. Taheri, J. Wang, Y. Yang, et al., *Nat. Nanotechnol.* **12**, 757 (2017).
- [20] L. Xu, M. Yang, L. Shen, J. Zhou, T. Zhu, and Y. P. Feng, *Phys. Rev. B* **97**, 041405 (2018).
- [21] T. C. Hsieh, M. Y. Chou, and Y. S. Wu, *Phys. Rev. Mater.* **2**, 034003 (2018).
- [22] T. Norden, C. Zhao, P. Zhang, R. Sabirianov, A. Petrou, and H. Zeng, *Nat. Commun.* **10**, 4163 (2019).
- [23] T. Y. T. Hung, K. Y. Camsari, S. Zhang, P. Upadhyaya, and Z. Chen, *Sci. Adv.* **5**, eaau6478 (2019).
- [24] D. Gut, M. Prokop, D. C. Sticlet, and M. P. Nowak (2019), arXiv: 1909.13738.
- [25] I. Appelbaum, B. Huang, and D. J. Monsma, *Nature* **447**, 295 (2007).
- [26] J. S. Moodera, T. S. Santos, and T. Nagahama, *J. Phys. Condens. Matter* **19**, 165202 (2007).
- [27] B. C. Huang, F. W. Chen, Y. C. Chen, and G. Y. Wu, *J. Appl. Phys.* **125**, 145701 (2019).
- [28] J. J. P. Thompson, D. J. Leech, and M. Mucha-Kruczyński, *Phys. Rev. B* **99**, 085420 (2019).
- [29] L. Majidi, M. Zare, and R. Asgari, *Solid State Commun.* **199**, 52 (2014).
- [30] H. Rostami and R. Asgari, *Phys. Rev. B* **91**, 075433 (2015).
- [31] M. Tahir, P. Vasilopoulos, and F. M. Peeters, *Phys. Rev. B* **93**, 035406 (2016).
- [32] V. Heine, *Phys. Rev.* **138**, 1689 (1965).
- [33] J. Tersoff, *Phys. Rev. Lett.* **52**, 465 (1984).
- [34] M. G. Reuter, *J. Phys.: Condens. Matter* **29**, 053001 (2017).
- [35] E. O. Kane, *J. Appl. Phys.* **32**, 83 (1961).
- [36] D. Szczęśniak, A. Ennaoui, and S. Ahzi, *J. Phys.: Condens. Matter* **28**, 355301 (2016).
- [37] D. Szczęśniak, R. D. Hoehn, and S. Kais, *Phys. Rev. B* **97**, 195315 (2018).

- [38] G. B. Liu, W. Y. Shan, Y. Yao, W. Yao, and D. Xiao, Phys. Rev. B **88**, 085433 (2013).